Catalysis Science & Technology

PAPER

View Article Online
View Journal | View Issue



Cite this: *Catal. Sci. Technol.*, 2016, **6**, 5737

# Plastically deformed Cu-based alloys as high-performance catalysts for the reduction of 4-nitrophenol†‡

Eredzhep Menumerov,§ Kyle D. Gilroy,§¶ Maryam Hajfathalian, Colin J. Murphy, Erica R. McKenzie, Robert A. Hughes and Svetlana Neretina*

Received 1st April 2016,
Accepted 19th April 2016

DOI: 10.1039/c6cy00734a

www.rsc.org/catalysis

The severe plastic deformation of metals leads to the formation of nanotextured surfaces as well as the retention of significant strain energy, characteristics which are known to promote catalytic activity. Here, we demonstrate plastically deformed surfaces of copper and copper-based alloys as being highly catalytic using the well-studied model catalytic reaction which reduces 4-nitrophenol to 4-aminophenol by borohydride. Among the materials studied, the most catalytically active is formed in a two-step process where metal chips are mechanically sheared from a Cu–Sn alloy containing precipitates and then exposed to an etchant which removes the precipitates from the exposed surface. The so-formed structures exhibit exceedingly high catalytic activity and set new benchmarks when incorporated into a fixed-bed reactor. The formation of catalytically active sites is shown to be strongly dependent on the presence of the precipitates during the deformation process, achieving an order of magnitude increase in the reaction rate constant when compared to similarly formed Cu–Sn catalysts lacking these precipitates. The work, therefore, demonstrates a new approach for generating catalytically active sites which may be applicable to other alloy combinations.

## Introduction

While the catalytic activity stemming from high-surface-area-to-volume structures with sub-15 nm dimensions is well-documented,[1] the corresponding reaction rates per unit surface area do not necessarily exceed those of complex mesoscopic or monolithic structures exhibiting surfaces with a nanoscale roughness characterized by a high density of atomic steps, kinks, and undercoordinated atoms.[2–12] In a scenario where the higher catalytic activity of these complex surfaces offsets deficiencies in terms of a low surface-area-to-volume ratio there is the potential to advance an alternate catalytic platform which supersedes existing systems.

In addition to its technological relevance, the reaction which reduces 4-nitrophenol (4-NP) to 4-aminophenol (4-AP) by borohydride serves as an important model reaction for assessing metallic nanostructures as catalytic materials. Consequently, there exists a vast literature commenting on the advantages and disadvantages of various catalytic materials and their supports.[13,14] From a practical standpoint, numerous factors come into play when assessing a catalyst including mass and specific catalytic activities, price, weight, durability, recoverability, selectivity, and ease of fabrication. A mechanistic understanding of what constitutes a highly catalytic surface for the reduction of 4-NP, however, is most readily obtained from a determination of the reaction rate constant per unit surface area of catalyst (*i.e.*, $k_{app}$/area). While such a metric is of obvious significance, it is rarely reported and, from an experimental standpoint, difficult to determine accurately. As a result, it is often equally difficult to ascertain whether high reaction rates arise from an intrinsically active surface or the large total surface area attainable when using an ensemble of small nanoparticles.

The plastic deformation of metals provides the means to transform a nominally flat metallic surface into one which undulates on length-scales which depend upon the mechanical forces applied.[15,16] Metals yield plastically when the applied load perturbs the strain fields of dislocations to the extent that they propagate though the material along slip bands, often intersecting with the surface and, hence, distorting it, a process which inevitably leads to a surface with steps, kinks, and undercoordinated atoms. Moreover,

*College of Engineering, Temple University, Philadelphia, Pennsylvania, 19122, USA. E-mail: neretina@temple.edu*

† The authors declare no competing financial interests.

‡ Electronic supplementary information (ESI) available: Videos showing the fixed-bed reactor in operation; catalyst preparation conditions; additional catalyst characterization. See DOI: 10.1039/c6cy00734a

§ These authors contributed equally.

¶ Current Address for K. D. G: The Wallace H. Coulter Department of Biomedical Engineering, Georgia Institute of Technology and Emory University, Atlanta, Georgia 30332, USA.

these same mechanical forces can lead to the generation of new dislocations which can respond likewise. The catalytic activation of metal surfaces through elastic and plastic deformation has long been recognized.[17–20] With nanoscale control over the strains at lattice-mismatched heteroepitaxial interfaces in core–shell and bimetallic nanoparticles being increasingly realized, there is renewed interest in manipulating these elastic strains to promote optimum catalytic behavior[21–27] as prescribed by volcano plot concepts and Sabatier's principle.[28] No such resurgence in interest, however, currently exists for the case of plastic deformation, although it could play an important role in the formation of the dealloyed ligaments which make up nanoporous Au catalysts.[29–32] Here, we demonstrate that the catalytic activity of Cu-based metals can be intensified through plastic deformation and, when suitably combined with an etching procedure, exhibit catalytically active surfaces which, in most cases, outperform nanoscale catalysts in the reduction of 4-NP when evaluated in terms of specific catalytic activity (*i.e.*, $k_{app}$/area). The so-formed catalysts are both inexpensive and easily fabricated and, when incorporated into a fixed-bed system for continuous-flow reactions, are able to outperform their nanoscale counterparts by a wide margin.

## Results and discussion

### Catalytically activating single crystals of Cu through plastic deformation

The mechanical activation of Cu surfaces through plastic deformation was first assessed using polished single crystals. While such samples are impractical from the standpoint of applications, their use here allows for a more definitive assignment of the catalytically active sites since the confounding influence of grain boundaries is removed. Fig. 1a–c shows scanning electron microscopy (SEM) images of the surfaces of [100]-, [110]-, and [111]-oriented crystals after being plastically bent around a cylindrical surface with a radius of curvature of 2 cm. All of the surfaces exhibit the characteristic linear features associated with slip bands in face centered cubic crystals. Such features originate from the propagation and subsequent intersection of numerous edge dislocations with the crystalline surface in response to an externally applied load. The ordered nature of the surface reconstruction originates from a strong tendency toward slippage of the {111} close-packed planes in a <110> direction. The geometric patterns formed by the slip bands for the different crystallographic orientations, therefore, correspond to the directions by which {111} planes intersect the various surfaces.

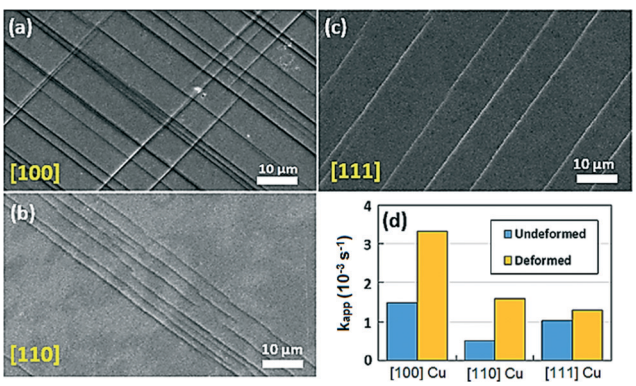


Fig. 1 SEM images of the slip bands formed on the surface of bent single crystals of (a) [100]-, (b) [110]-, and (c) [111]-oriented Cu. (d) Histogram showing $k_{app}$ values for the reduction of 4-NP for each orientation before and after deformation.

The assessment of catalytic activity for both the as-received and plastically deformed surfaces toward the reduction of 4-NP was made using well-established spectroscopic techniques,[13,14] where the Cu crystals were deployed using a dip catalyst modality.[33–35] The results reveal an enhancement to the reaction rate constant, $k_{app}$, resulting from plastic deformation for all orientations (Fig. 1d). It demonstrates that the plastic deformation of Cu gives rise to catalytically active surface sites in the absence of grain boundaries irrespective of the crystallographic surface orientation. It should, however, be recognized that grain boundary influences may heighten catalytic activity when using polycrystalline materials.[36–38]

### Catalytically activating Cu and Cu-based alloys through a shear deformation

While the single crystal results demonstrate the viability of plastic deformation in forming catalytically active sites, it should be understood that these materials have undergone a relatively mild deformation where only a small percentage of the surface shows the distinctive morphology resulting from the propagation of edge dislocations to the surface. By cold working Cu to the point where it has undergone severe plastic deformation it is possible to increase the edge dislocation density at the surface from approximately $10^8$ to $10^{12}$ $cm^{-2}$,[39] a process which completely transforms the surface morphology. Moreover, the type of deformation (*e.g.*, bending, rolling, shearing) as well as the conditions under which it is carried out can be crucial in determining the exact nature of the surface. One of the most severe forms of plastic deformation occurs when a machine tool cuts a metal. The cutting action, shown schematically in Fig. 2a, originates from the compression and subsequent shear along a plane from which highly deformed metal chips emerge. The concave surface of the chip exhibits a serrated surface morphology (Fig. 2b) while the convex surface is relatively smooth (Fig. 2c) due to secondary deformations occurring as the machine tool passes over the sheared surface. Ductile metals, such as Cu, give rise to long semi-continuous chips (or turnings) while semi-ductile metals, such as brass and bronze, frequently fracture into short segments (Fig. 2d). It is these highly deformed metal chips which are assessed as catalytic materials for the reduction of 4-NP.

In a demonstration of their catalytic capabilities, plastically deformed chips of copper, brass (Cu : Zn : Pb = 61.5 :

 

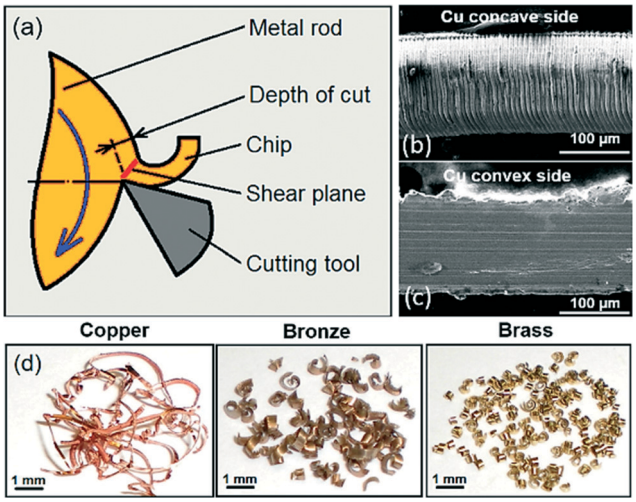


Fig. 2 (a) Schematic illustrating the process by which metal is sheared from a rotating solid rod in contact with a stationary cutting tool. SEM images showing the (b) nanostructured concave and (c) convex surfaces of plastically deformed Cu chips. (d) Optical images of semi-continuous Cu chips and highly segmented bronze and brass chips.

36.5 : 2 wt%), and bronze (Cu : Sn : Pb = 81 : 7 : 12 wt%) were loaded into a 10 mm inner diameter column to a height of 8.5 cm and used as a fixed-bed catalyst in a continuous-flow reactor (Fig. 3a). When optimized, reactants containing 4-NP and $NaBH_4$, which appear yellow in color, percolate through the catalyst and exit as a clear liquid containing the 4-AP product. Such systems allow for sustained uninterrupted reactions,[40–42] a modality which is highly desirable in a manufacturing setting.[43] With the goal of reducing all of the 4-NP at the highest possible concentration and flow rate, the fixed bed reactor was optimized for each catalyst by adding 4-NP with molarities of up to 30 mM in 5 mM increments.

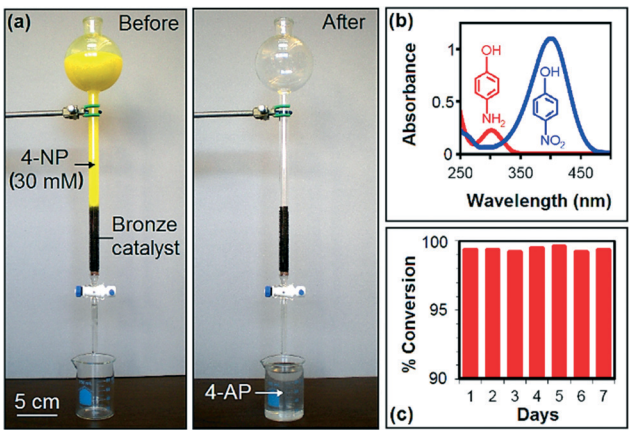


Fig. 3 (a) Fixed-bed system for continuous-flow catalysis where 100 mL of the reactants containing 30 mM 4-NP (yellow liquid) percolate through the bronze catalyst and emerge as a clear liquid containing the 4-AP product. (b) Absorbance spectra showing the characteristic 400 nm 4-NP peak in the reactants (blue) and the 300 nm 4-AP peak in the product (red). (c) Percent conversion to 4-AP observed over 7 reaction cycles carried out on consecutive days where 100 mL of solution was flowed through the column per day.

The reported molarities and flow rates are those which are sustainable without unreacted 4-NP appearing in the product. The reduction of 4-NP to 4-AP was verified through spectroscopic measurements (Fig. 3b) which reveal that the prominent 400 nm peak associated with 4-NP, while present in the reactants, is absent in the product. It is replaced with a 300 nm peak which is the spectroscopic signature of the 4-AP product. Each catalyst tested was able to maintain the same performance over a 7 day period (Fig. 3c, also see Fig. S1, ESI‡), providing evidence that these catalysts are long-lived. SEM and EDS measurements performed on the used catalysts showed no obvious signs of deterioration.

When plastically deformed Cu was loaded into the fixed-bed reactor it was able to reduce 10 mM of 4-NP at a flow rate of 13 mL $min^{-1}$. The performance of the brass catalyst was relatively poor in that comparable flow rates could only be achieved if a 5 mM 4-NP solution was used. This result indicates that alloying Cu with Zn is detrimental to catalytic activity. Conversely, the bronze catalyst outperformed Cu, achieving a maximum flow rate of 16 mL $min^{-1}$ at a 4-NP concentration of 10 mM. While the bronze catalyst showed the highest level of catalytic activity, inductively coupled plasma mass spectrometry (ICP-MS) performed on the 4-AP product revealed Cu, Sn, and Pb levels of 2230, 67.9 and 1810 μg $L^{-1}$, respectively. With high levels of Pb being particularly undesirable we explored options to reduce contamination levels. Pb exists in bronze as an immiscible component expelled from the surrounding Cu–Sn alloy as a precipitate during the solidification process. When bronze is machined Pb acts as a lubricant due to its low shear strength.[44] By exposing the bronze chips to nitric acid prior to their insertion into the fixed-bed reactor the Cu, Sn, and Pb levels were reduced to 1010, 59.2 and 248 μg $L^{-1}$, respectively. Of far greater importance were the significant enhancements to catalytic activity induced by the etching process, allowing for a higher flow rate (23 mL $min^{-1}$) at double the 4-NP concentration (*i.e.*, 20 mM) or, alternatively, the reduction of 30 mM 4-NP at a flow rate of 15 mL $min^{-1}$. Noteworthy is that this 4-NP concentration is 300-times greater than that which is typically used when spectroscopically assessing nanoparticle catalysts (*i.e.* 100 μM). A further 3-fold increase in the flow rate to 63 mL $min^{-1}$ at 20 mM 4-NP was achieved by applying suction to the reactor output. Videos S1a and b in the ESI‡ show the operating reactor under suction and when no suction is applied, respectively. It is noteworthy that these results were achieved with metal chips produced in under 5 min at a material cost of 6¢. Cu and brass show only minor enhancements to catalytic activity when exposed to the same etching procedure.

The validation of a fixed-bed catalytic reactor using plastically deformed and etched bronze provides a proof-of-concept demonstration that such bulk-scale materials are amenable to continuous-flow catalysis. Other examples of fixed-bed reactors have been recently demonstrated using supported nanostructures as the catalyst.[37–39] Of these, the system validated by He *et al.*[40] based on Au nanowire

catalysts affixed to glass fiber supports, shows the most impressive capabilities. The bronze catalyst is, however, able to react 4-NP at twice the rate under both evacuated and regular flow conditions, a result which attests to the viability of using plastic deformation as a means to fabricate catalytically active surfaces. Additional advantages which these catalysts have over their nanoscale counterparts include: (i) the elimination of difficulties associated with catalyst anchoring and aggregation,[40] (ii) a catalyst fabrication process which is free of ligands which can inhibit the catalytic activity of nanoparticles[45–47] and are a potential product contaminant, (iii) a catalyst synthesis which is rapid, inexpensive, and scalable, and (iv) the use of bronze which, when compared to current nanoscale catalysts such as Au and Pd, is far more cost-effective. In fact, bronze chips are already produced in large quantities as a byproduct of manufacturing processes; their use as a catalyst provides the prospect of using what is nominally a waste product as a functional material.

### Characterization of the Cu–Sn alloy catalyst

With the plastic deformation and subsequent etching of bronze showing the most favorable catalytic properties, a set of experiments were performed in order to elucidate the mechanisms responsible for the catalytic activity. For these experiments 100 mg of catalyst was used. While this value may seem large compared to the mass of nanoscale catalysts commonly used for this reaction, the total catalyst surface area is smaller than what is typical since these mesoscopic catalysts have a relatively low surface-area-to-volume ratio. The degree of catalytic enhancement resulting from the etching process was quantified by placing the catalyst into a cuvette containing 2 mL of 100 μM 4-NP while spectroscopically monitoring the fall in the 400 nm 4-NP absorbance resulting from its conversion to 4-AP. Fig. 4a shows the time-dependent absorbance for the unetched bronze catalyst from which an apparent reaction rate constant ($k_{app}$) of $6 \times 10^{-4}$ $s^{-1}$ was derived from the slope of the $-\ln(A(t)/A(t_o))$ *vs.* time plot (Fig. 4b). The same bronze chips were then etched in 2 M nitric acid for 10 min and, when reassessed as catalysts, achieved a $k_{app}$ value of $8 \times 10^{-2}$ $s^{-1}$ (Fig. 4c and d), a more than two order of magnitude improvement. When this $k_{app}$ value is normalized to the total surface area of the etched catalyst (estimated to be $2.4 \times 10^{-4}$ $m^2$) a $k_{app}$/area value of 330 $s^{-1}$ $m^{-2}$ is obtained. The dependency of $k_{app}$ on the reaction temperature was also assessed for temperatures between 15 and 45 °C. A plot of $\ln(k_{app})$ *vs.* $T^{-1}$ shows a linear dependency (see Fig. S2, ESI‡) in accordance with Arrhenius behavior from which an activation energy of 42 kJ $mol^{-1}$ is derived. The result compares well to the 49 kJ $mol^{-1}$ value obtained by Wunder *et al.* for Au nanoparticles.[48]

In an effort to determine if the plastically deformed bronze surface compares well to its nanoscale counterparts in terms of the $k_{app}$/area metric, we compiled from the literature a list of competing values based on the information provided. It is noted that a significant number of reports do not provide sufficient information to calculate this value and were, hence, excluded on this basis. Table 1 lists only those catalysts which achieved a $k_{app}$/area value of greater than 10 $s^{-1}$ $m^{-2}$ and is, hence, a list of the top performing catalytic surfaces from the standpoint of this catalytic descriptor. We wish to stress that this descriptor, while providing information of relevance in obtaining a mechanistic understanding, does not necessarily translate into a catalyst of practical importance since other factors must be considered. Evident is that some of the highest values occur for catalysts which: (i) are comprised of alloys of Cu,[33,49–51] (ii) have ligand-free[33,45] or dendrimer coated[51,52] surfaces, and (iii) exhibit low coordination surface sites in such forms as high-index facets, high-curvature geometries, and/or an abundance of atomic surface steps.[33,49–51] Also evident is that the bronze catalyst is among this list of the most catalytically active surfaces ever prepared for the reduction of 4-NP. This, from a mechanist standpoint, indicates that the plastic deformation and etching procedure gives rise to catalytically active sites which are more active and/or more numerous than most nanomaterials.

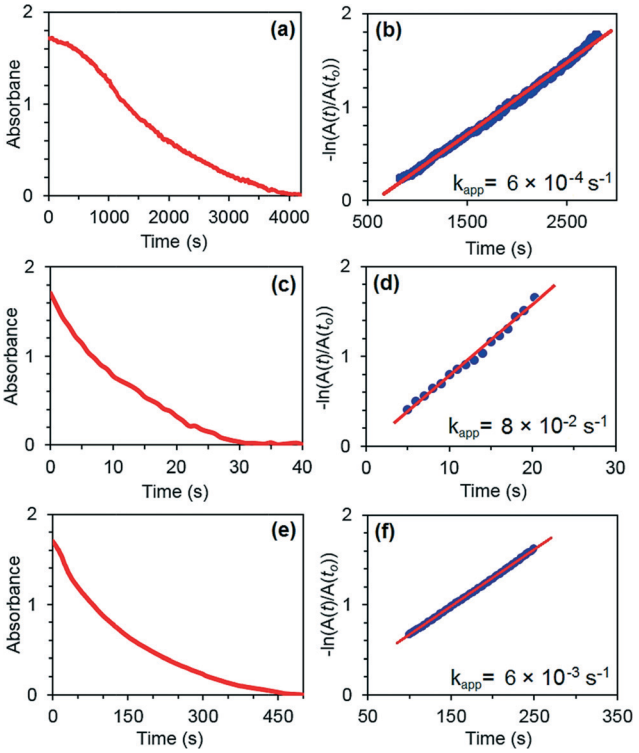


Fig. 4 Time-dependence of the 400 nm 4-NP absorbance and the corresponding $-\ln(A/A_o)$ *vs.* time plot, from which the apparent reaction rate constant, $k_{app}$, is extracted for (a–b) an unetched bronze catalyst, (c–d) an etched bronze catalyst, and (e–f) an etched Pb-free bronze catalyst. Note that the time-axis varies greatly for the various samples.

Attempts to induce similar catalytic activity in a Pb-free bronze (Cu : Sn : P = 94.8 : 5 : 0.2 wt%) using plastic deformation proved unsuccessful, achieving a $k_{app}$ value of only $5 \times 10^{-3}$ $s^{-1}$ when plastically deformed, which, when etched, rose slightly to $6 \times 10^{-3}$ $s^{-1}$ (Fig. 4e and f). When normalized to

 

**Table 1** A comparison of the reaction rate constant normalized to the catalyst surface area for various catalytic platforms

| Catalytic platform | Material | Surface | Particle shape | Dimension | $k_{app}$/area[a,b] ($s^{-1}$ $m^{-2}$) |
|---|---|---|---|---|---|
| Sub-15 nm nanoparticles | Au ref. 52 | Dendrimer | Spherical | dia. = 3.1 nm | 254 |
| | Ag ref. 52 | Dendrimer | Spherical | dia. = 3.1 nm | 238 |
| | Au ref. 54 | CTAB | Spherical | dia. = 13 nm | 104 |
| | Au ref. 45 | Ligand-free | Spherical | dia. = 7.2 nm | 57 |
| | Pd ref. 53 | Dendrimer | Spherical | dia. = 3.0 nm | 11 |
| Complex nanostructures | $AuCu_3$ ref. 49 | Amine | Nanorod | ($l$, $w$) = (27, 10 nm) | 525 |
| | AuCu ref. 51 | Oleyamine | Hollow nanorod | ($l$, dia, wall) = (35, 12, 2 nm) | 205 |
| | Au ref. 55 | PVP | Hollow nanocube cages | (edge, wall) = (50, 5 nm) | 199 |
| | AuCu ref. 50 | HDA | Pentacle stars | (arm, core) = (20, 25 nm) | 87 |
| | Au–Pt ref. 56 | CTAB | Cylindrical dumbbells | ($l$, dia) = (7.4, 39.5 nm) | 42 |
| | AuCu ref. 33 | Ligand-free | Hemispherical | dia. = 100 nm | 17 |
| Plastically deformed and etched[c] | Bronze | Ligand-free | Chips | ($l$, $w$, $h$) = (2.9, 0.2, 0.05 mm) | 330 |

[a] All values estimated based on the information provided in the cited references. [b] The concentrations of the reactants and the amount catalyst used vary among these measurements. [c] Values derived from this work.

the catalyst surface area a $k_{app}$/area value of only 19 $s^{-1}$ $m^{-2}$ is obtained, but which is still among the most catalytically active materials for this reaction. The implications of these results are (i) that the plastically deformed Cu–Sn alloy is highly catalytic toward the reduction of 4-NP, but where the presence of Pb precipitates during the deformation leads to far greater catalytic activity, and (ii) that the etching procedure is of significance only when Pb is present.

Fig. 5a shows SEM images and the corresponding elemental maps for the serrated concave surface of the bronze chips before and after 10 min of etching (see Fig. S3, ESI‡ for the corresponding data for the convex surface). This analysis revealed that Pb tends to collect at the leading edge of the serrations (denoted by the green arrow) or remain as embedded precipitates (red arrow). Horizontal tracks of Pb smeared across the surface by the cutting tool are also visible (blue arrows). Etching removes the Pb from these surfaces, leaving behind exposed edges and pits (yellow arrows). While the overall morphology of the etched surface is somewhat rougher, the gain in surface area is decidedly insufficient to account for the more than 133-fold increase in $k_{app}$. The results strongly suggest that the vast majority of the catalytic sites are initially coated with a relatively inert layer of Pb which, when removed, are exceedingly active.

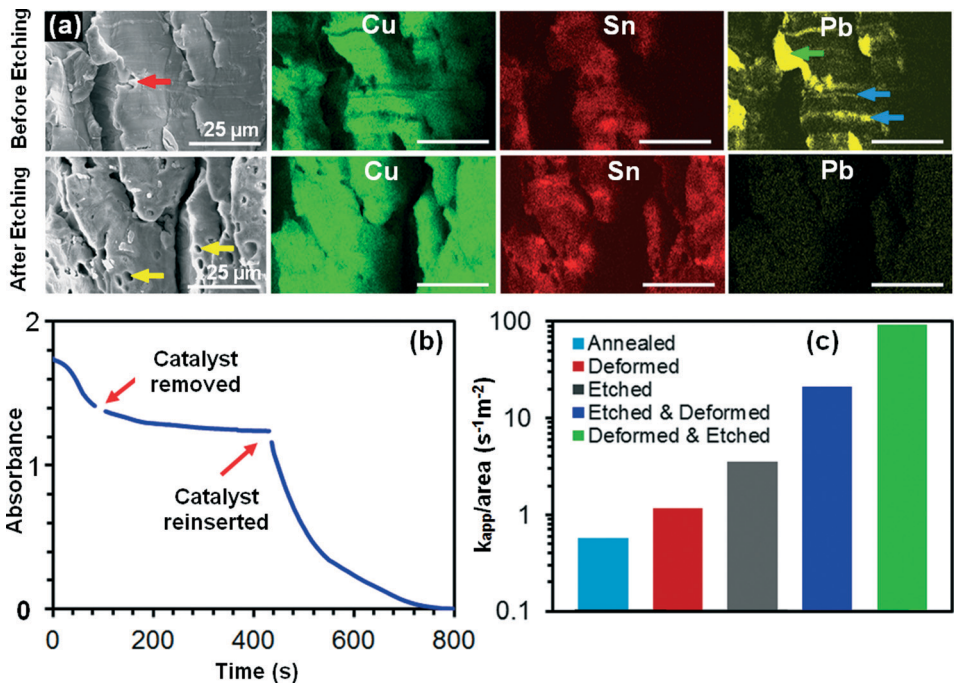


**Fig. 5** (a) SEM images and the associated elemental maps of plastically deformed bronze chips before and after being exposed to a nitric acid etch. (b) Time dependence of the 4-NP absorbance obtained when the reaction is terminated and then restarted through the removal and subsequent reinsertion of a bronze catalyst (plastically deformed and etched) into the 4-NP solution. (c) Histograms of the $k_{app}$ values normalized to the surface area of bulk bronze samples which have been subjected to various processing conditions.

Further mechanistic insights were obtained by preparing identical bulk bronze samples ($7 \times 7 \times 1.5$ mm$^3$) which could then be subjected to plastic deformations and etching processes. In all cases, the samples were first annealed at 300 °C to limit any catalytic activity associated with the initial sample preparation. When plastic deformation was carried out, it was through a bending deformation. These bulk samples allowed for easy removal from the cuvette midway through the reaction followed by reinsertion at a later time. Fig. 5b shows the time-dependent absorbance of a bronze catalyst as this procedure is carried out. The fact that the reaction terminates when the catalyst is removed confirms that it is the bronze surface, and not leached material, which is catalytic. The influence of processing conditions on the reaction rate constant is summarized by the histogram shown in Fig. 4c. Note that the wide variation in the $k_{app}$/area values necessitate the use of a logarithmic scale. The annealed sample is, as expected, a relatively poor catalyst. Moderate increases are experienced when samples are either etched or bent, but not both. The combination of etching and bending, however, gives rise to dramatic increases in $k_{app}$ where a bending-etching process shows a more than 4-fold enhancement over the reverse etching-bending sequence. The results support the conclusion that the formation and/or activity of the catalytic sites is enhanced, not solely through etching, but when the immiscible Pb precipitates are present within the Cu–Sn alloy during plastic deformation.

### Mechanistic drivers for the catalytic activity

The assembled results point toward three factors of significance when forming highly catalytic Cu–Sn surfaces: (i) plastic deformation, (ii) the presence of Pb precipitates within the alloy matrix, and (iii) the etching procedure. While a comprehensive mechanistic understanding is unattainable from this initial study, it is possible to speculate on the roles played by each these three factors. With all of the materials studied showing increased catalytic activity toward the reduction of 4-NP, it has been unequivocally demonstrated that plastic deformation leads to the formation of active sites. This activity likely stems from the deformation-induced surface reconstruction which gives rise to a disorganized nanotextured surface with a high density of steps, kinks, and undercoordinated atoms. Such features are widely acknowledged as being conducive to catalytic activity. While most of the energy used in the deformation process is dissipated as heat (>90%),[16] the retention of strain energy within the crystal lattice could also contribute to the catalytic activity.[21–27]

With plastically deformed elemental Pb showing no catalytic activity toward the reduction of 4-NP (see Fig. S5a, ESI‡), it is not surprising that its removal through etching leads to a more catalytic surface. This, however, does not account for the more than one order of magnitude difference in $k_{app}$ between etched bronze and its Pb-free counterpart (Fig. 4c–f). This dissimilarity likely originates from the fact that the deformation process is fundamentally altered when Pb-precipitates are present in the alloy matrix; their impact on the shear deformation process (*i.e.*, their machinability) is, in fact, the reason they are added to this particular alloy.[44] Such differences could direct the deformation process toward a surface which is more active. Precipitates within an alloy matrix also tend to act as impediments to edge dislocation motion. With the resulting dislocation pile-up at the precipitate boundary giving rise to significant lattice strains, it is conceivable that such strains may be conducive to the formation of catalytic sites.

While the role of the etching procedure may simply be to remove catalytically inactive Pb from the surface, it is difficult to rule out other possibilities. Etching procedures, specifically those which preferentially remove one component of an alloy (*i.e.*, dealloying), are well-established as a means to promote catalytically activity.[2–9] The etching procedure used, while removing Pb from the surface, also leads to the loss of Cu as is evident from a color change in the etching solution which begins after $2\frac{1}{2}$ min and transforms it from transparent to the characteristic blue color associated with solvated $Cu^{2+}$ ions. In addition, when much longer etching times than those used to produce the Cu–Sn catalyst are carried out (>60 min), the surface appears Sn-rich. While such factors point toward dealloying as a mechanistic driver of significance, there are arguments to be made against this possibility. Foremost, is the fact that the Pb-free bronze shows little improvement in $k_{app}$ after it has undergone the same etching procedure (before: $5 \times 10^{-3}$ s$^{-1}$, after: $6 \times 10^{-3}$ s$^{-1}$) even though it should experience similar levels of dealloying. The fact that plastically deformed elemental Sn, by itself, shows essentially no catalytic activity toward the reduction of 4-NP (see Fig. S5b, ESI‡) further argues against this possibility. It is also noted that the 10 min etch times and acid concentrations used to activate the Cu–Sn catalyst are much smaller than those typically used when dealloying materials. In addition, the highly porous morphologies expressed by dealloyed materials[2–9] do not resemble those of the etched catalyst (Fig. 5a). Nevertheless, it is impossible at this stage to rule out etching-induced surface alterations as a means to generate catalytically active sites, a scenario whose likelihood becomes more probable if the sites are formed through synergistic processes requiring the exposure of a strained surface to an etchant. Such synergies may, in fact, be partially responsible for the high catalytic activity displayed by nanoporous Au since the dealloying process is accompanied by a spontaneous plastic deformation.[39–42]

## Conclusion

In summary, we have demonstrated that the plastic deformation of a Cu–Sn alloy with Pb precipitates followed by an etching procedure renders its surface highly catalytic toward the reduction of 4-NP. Such surfaces compare favorably to the top performing nanoscale catalysts when benchmarked using the reaction rate constant normalized to the surface area of the catalyst. The catalysts are easily fabricated and are

 

demonstrated as inexpensive, robust, highly recyclable, and amenable to continuous-flow catalytic reactions. The results strongly suggest that the presence of Pb precipitates within the Cu–Sn alloy matrix during the deformation is highly conducive to the formation of catalytically active sites. These plastically deformed surfaces join a class of bulk-scale materials such as dealloyed metals, RANEY® catalysts, and various sponge-like materials, where catalysis occurs on disorganized surfaces with a high density of steps, kinks, and undercoordinated atoms. The work opens up the possibility of using similarly formed catalytic materials in a broad range of reactions driven by the alloy combination deemed most effective.

# Experimental

### Chemicals and materials

(111)-, (110)-, and (100)-oriented single crystals of Cu with a purity greater than 99.99% were purchased from MTI Corp. The crystals, which have dimensions of 10 × 10 × 0.5 mm, are one-side polished with an RMS roughness of less than 30 Å. The catalytic materials were derived from solid rods of C110 copper, C353 brass (Cu : Zn : Pb = 61.5 : 36.5 : 2 wt%), C936 bronze (Cu : Sn : Pb = 81 : 7 : 12 wt%) and C510 bronze (Cu : Sn : P = 94.8 : 5 : 0.2 wt%) with a diameter of 2.54 cm. Catalyst etching procedures utilized nitric acid (Sigma Aldrich). Annealing regimens were carried out in ultra-high purity (UHP) Ar. Solutions for catalysis were prepared using 4-NP (Fluka), $NaBH_4$ (Fluka), and deionized (DI) water derived from a Milli-Q system (18.2 MΩ cm at 25 °C).

### Sample preparation through plastic deformation and etching

**The plastic deformation of single crystals of copper.** Prior to use as a catalyst, both the unpolished and side surfaces of the single crystals were coated with a lacquer in order to render these surfaces catalytically inactive. All catalytic activity could, hence, be attributed to the single exposed polished surface (see Fig. S4, ESI‡). The bending deformation around a nylon surface with a radius of curvature of 2 cm was carried out using bending pliers. After deformation a second layer of lacquer was applied in order to ensure that the unpolished and side surfaces remained catalytically inactive.

**The fabrication of plastically deformed metal chips of copper, bronze, and brass.** The metal chips of copper, bronze, and brass which were used as catalysts in the fixed-bed continuous-flow reactor (Fig. 3a) were formed using the shearing forces which a tungsten carbide cutting tool exerted on a rotating metal rod. The parameters used in the shearing process were optimized for each metal (see Table S1, ESI‡) to yield the maximum catalytic activity using 100 mg sample sizes. Etching procedures were carried out in 2 M nitric acid under gentle stirring followed by a thorough rinse in DI water.

**The fabrication of bulk bronze samples for mechanistic studies.** The bulk bronze catalysts, with dimensions of 7 × 7 × 1.5 $mm^3$, which were used to generate the data in Fig. 5b and c were all cut from the same metal rod used to fabricate the metal chips for the fixed-bed reactor. Once cut, the surfaces were polished and annealed in order to minimize any catalytic activity stemming from the cutting process. The annealing regimen saw the samples heated to 300 °C for 2 h in a tube furnace where Ar was flowed at a rate of 60 sccm.

### Catalysis measurements

**Catalysis on Cu single crystals and bulk bronze samples.** All absorbance spectra were obtained for reactions carried out in a 1 cm path length quartz cuvette containing a 2 mL aqueous solution of the 4-NP (100 μM) and $NaBH_4$ (10 mM) reactants. The surface area of the 100 mg bronze sample, form which the $k_{app}$/area values were obtained, was estimated from SEM measurements on 20 bronze chips of known weight. The estimate was conservative in that the calculation accounted for the surface roughness by assuming that each striation penetrated through the through the entire thickness of the chip even though this exaggerated the result. No allowances were made for the fact that a substantial portion of the catalyst surface area is resting on the bottom cuvette and is, hence, shielded from the 4-NP solution.

**Catalysis using the fixed-bed catalytic reactor.** The apparatus used to demonstrate continuous flow catalysis was intentionally designed to mimic that used by He *et al.*[40] in order to facilitate comparisons with the many impressive benchmarks set when using Au nanorod catalysts affixed to glass fiber supports. The copper, bronze, and brass catalysts were all tested in the same apparatus, but where an emptied column was first cleaned by filling it with 150 mM nitric acid for at least 24 hours before switching materials. The column was then thoroughly flushed with DI water before adding the new catalyst. It was then filled to height of 8.5 cm with the catalyst material. Whenever fresh catalytic material was used, the product exiting from the reactor initially appeared discolored (grey to black), but then quickly turned clear. To circumvent these contamination issues, a conditioning process was adopted whereby fresh catalytic material was exposed to a 200 mL aqueous solution of 10 mM 4-NP and 1 mM $NaBH_4$ prior to collecting any data.

Once the conditioning process was complete, the reactor was optimized by trying to reduce the highest possible 4-NP concentration at the highest flow rate. For these experiments, the 4-NP concentration was increased in 5 mM increments to a maximum of 30 mM, where the 4-NP : $NaBH_4$ molar ratio was held constant at 1 : 100, a value which is typical for this reaction. Spectroscopic characterization of the reactants and product obtained were carried out in order to determine the 4-NP percent conversion (Fig. 3b and c). Prior to analysis the 4-NP and 4-AP concentrations were diluted by a factor of 300 and 100, respectively, in order to allow detectable levels of light to pass through the sample. Such dilutions are required because the concentrations used in the reactor are more than 100× greater than that which is typically used for a spectroscopic assessment of catalysts for the reduction of 4-NP.

The fixed-bed reactor was operated for a 7 day period for each of the catalysts assessed (*i.e.*, copper, brass, and bronze), whereby 100 mL of reactants were flowed at the maximum sustainable rate at least once per day. Between tests the column was filled with the 4-AP product since the long-term exposure of the drying catalysts to air led to a discoloration and diminished catalytic activity. The reactor was also operated with suction applied at the output in order to demonstrate the faster flow rates achievable when using the plastically deformed and etched bronze catalyst. High flow rates are facilitated by the greater pressure differential created between the input and output of the reactor.

### ICP-MS measurements

The 4-AP product derived from the fixed-bed catalytic reactor was analyzed for Cu, Sn, and Pb using ICP-MS. The samples used were acquired after, at least, 300 mL of reactants had been flowed through the fixed-bed reactor. They were then diluted by a factor of 100 with DI water. The test tubes for ICP-MS analysis were three times acid washed with 150 mM $HNO_3$ and 5 times rinsed with DI water. Metal analysis was conducted on acidified samples (1% $HNO_3$) using an Agilent 7900 inductively coupled plasma mass spectrometer (ICP-MS). Before each use, the instrument was tuned to minimize oxides and double charged ions; He gas was included in the collision cell to minimize polyatomic interferences. Samples were diluted as needed to ensure accurate analysis and internal standards were employed to account for matrix effects. Triplicate samples were analyzed for each treatment and reproducibility was high among replicates. Cu and Sn were monitored at multiple mass peaks, and data is presented from the mass with the least interference. Presented Pb concentrations are the summation of three isotopes (206, 207, and 208). Detection limits were analyte and run specific, but were generally less than 1 $\mu g\ L^{-1}$.

### Instrumentation

SEM images and EDS elemental maps were obtained using a 450 FEG ESEM environmental scanning electron microscope in secondary electron mode. The spectroscopic assessment of catalytic processes was carried out using a Jasco UV/Vis Spectrophotometer V630. An Agilent 7900 ICP-MS was used to determine the levels of Cu, Sn, and Pb in the 4-AP product. Annealing procedures were carried out in a Lindberg Blue M furnace equipped with a quartz tube and the fittings needed to maintain a continuous flow of UHP Ar gas.

## Acknowledgements

This work is funded by the National Science Foundation awards (DMR-1053416 and DMR-1505114) to S. Neretina. It has also benefited from the facilities available through Temple University's Nano Instrumentation Center as well as the expertise of D. A. Dikin (Facility Manager). K. D. G. acknowledges helpful discussions with Dr. Eric Borguet (Chemistry, Temple University) and support received through a Temple University Graduate Student Fellowship.

## References

1 E. Roduner, *Chem. Soc. Rev.*, 2006, **35**, 583–592.
2 J. Biener, M. M. Biener, R. J. Madix and C. M. Friend, *ACS Catal.*, 2015, **5**, 6263–6270.
3 X. Zhang and Y. Ding, *Catal. Sci. Technol.*, 2013, **3**, 2862–2868.
4 A. Wittstock and M. Bäumer, *Acc. Chem. Res.*, 2014, **47**, 731–739.
5 L.-C. Wang, K. J. Stowers, B. Zugic, M. M. Biener, J. Biener, C. M. Friend and R. J. Madix, *Catal. Sci. Technol.*, 2015, **5**, 1299–1306.
6 T. Fujita, P. Guan, K. McKenna, X. Lang, A. Hirata, L. Zhang, T. Tokunaga, S. Arai, Y. Yamamoto, N. Tanaka, Y. Ishikawa, N. Asao, Y. Yamamoto, J. Erlebacher and M. Chen, *Nat. Mater.*, 2012, **11**, 775–780.
7 A. Wittstock, V. Zielasek, J. Biener, C. M. Friend and M. Bäumer, *Science*, 2010, **327**, 319–322.
8 C. Xu, J. Su, X. Xu, P. Liu, H. Zhao, F. Tian and Y. Ding, *J. Am. Chem. Soc.*, 2007, **129**, 42–43.
9 V. Zielasek, B. Jürgens, C. Schulz, J. Biener, M. M. Biener, A. V. Hamza and M. Bäumer, *Angew. Chem., Int. Ed.*, 2006, **45**, 8241–8244.
10 J. Rosen, G. S. Hutchings, Q. Lu, S. Rivera, Y. Zhou, D. G. Vlachos and F. Jiao, *ACS Catal.*, 2015, **5**, 4293–4299.
11 Q. Lu, J. Rosen, Y. Zhou, J. S. Hutchings, Y. C. Kimmel, J. G. Chen and F. Jiao, *Nat. Commun.*, 2014, **5**, 3242.
12 J. R. Mellor, N. J. Coville, S. H. Durbach and R. G. Copperthwaite, *Appl. Catal., A*, 1998, **171**, 273–281.
13 P. Zhao, X. Feng, D. Huang, G. Yang and D. Astruc, *Coord. Chem. Rev.*, 2015, **287**, 114–136.
14 P. Hervés, M. Pérez-Lorenzo, L. M. Liz-Marzán, J. Dzubiella, Y. Lu and M. Ballauff, *Chem. Soc. Rev.*, 2012, **41**, 5577–5587.
15 Y. Z. Dai and F. P. Chiang, *J. Eng. Mater. Technol.*, 1992, **114**, 432–438.
16 R. Abbaschian, L. Abbaschian and R. E. Reed-Hill, *Physical Metallurgy Principles*, Cengage Learning, Stamford, 2009.
17 M. Gsell, P. Jakob and D. Menzel, *Science*, 1998, **280**, 717–720.
18 Z. Li, D. V. Potapenko and R. M. Osgood, *ACS Nano*, 2015, **9**, 82–87.
19 P. G. Fox, *J. Mater. Sci.*, 1975, **10**, 340–360.
20 R. Otero, F. Calleja, V. M. García-Suárez, J. J. Hinarejos, J. de la Figuera, J. Ferrer, A. L. Váquez de Parga and R. Miranda, *Surf. Sci.*, 2004, **550**, 65–72.
21 M. F. Francis and W. A. Curtin, *Nat. Commun.*, 2015, **6**, 6261.
22 P. Strasser, S. Koh, T. Anniyev, J. Greeley, K. More, C. F. Yu, Z. C. Liu, S. Kaya, D. Nordlund, H. Ogasawara, M. F. Toney and A. Nilsson, *Nat. Chem.*, 2010, **2**, 454–460.
23 A. Jha, D.-W. Jeong, J.-O. Shim, W.-J. Jang, Y.-L. Lee, C. V. Rode and H.-S. Roh, *Catal. Sci. Technol.*, 2015, **5**, 2752–2760.
24 L. Gan, M. Heggen, S. Rudi and P. Strasser, *Nano Lett.*, 2012, **12**, 5423–5430.

 

25 S. Zhang, X. Zhang, G. Jiang, H. Zhu, S. Guo, D. Su, G. Lu and S. Sun, *J. Am. Chem. Soc.*, 2014, **136**, 7734–7739.
26 J. X. Wang, H. Inada, L. Wu, Y. Zhu, Y. Choi, P. Liu, W.-P. Zhou and R. R. Adzic, *J. Am. Chem. Soc.*, 2009, **131**, 17298–17302.
27 M. Mavrikakis, B. Hammer and J. K. Nørskov, *Phys. Rev. Lett.*, 1998, **81**, 2819–2822.
28 J. K. Nørskov, T. Bligaard, B. Hvolbæk, F. Abild-Pederson, I. Chorkendorff and C. H. Christensen, *Chem. Soc. Rev.*, 2008, **37**, 2163–2171.
29 B.-N. D. Ngô, A. Stukowski, N. Mameka, J. Markmann, K. Albe and J. Weissmüller, *Acta Mater.*, 2015, **93**, 144–155.
30 J. Weissmüller, H.-L. Duan and D. Farkas, *Acta Mater.*, 2010, **58**, 1–13.
31 J. Weissmüller, R. C. Newman, H.-J. Jin, A. M. Hodge and J. W. Kysar, *MRS Bull.*, 2009, **34**, 577–586.
32 S. Parida, D. Kramer, C. A. Volkert, H. Rösner, J. Erlebacher and J. Weissmüller, *Phys. Rev. Lett.*, 2006, **97**, 035504.
33 M. Hajfathalian, K. D. Gilroy, A. Yaghoubzade, A. Sundar, T. Tan, R. A. Hughes and S. Neretina, *J. Phys. Chem. C*, 2015, **119**, 17308–17315.
34 E. Hariprasad and T. P. Radhakrishnan, *Chem. Eur. – J.*, 2010, **16**, 14378–14384.
35 G. Zheng, L. Polavarapu, L. M. Liz-Marzán, I. Pastoriza-Santos and J. Pérez-Juste, *Chem. Commun.*, 2015, **51**, 4572–4575.
36 A. Verdaguer-Casadevall, C. W. Li, T. P. Johansson, S. B. Scott, J. T. McKeown, M. Kumar, I. E. L. Stephens, M. W. Kanan and I. Chorkendorff, *J. Am. Chem. Soc.*, 2015, **137**, 9808–9811.
37 X. Feng, K. Jiang, S. Fan and M. W. Kanan, *J. Am. Chem. Soc.*, 2015, **137**, 4606–4609.
38 C. W. Li, J. Ciston and M. W. Kanan, *Nature*, 2014, **508**, 504–507.
39 L. E. Cratty, Jr. and A. V. Granato, *J. Chem. Phys.*, 1957, **26**, 96–97.
40 J. He, W. Ji., L. Yao, Y. Wang, B. Khezri, R. D. Webster and H. Chen, *Adv. Mater.*, 2014, **26**, 4151–4155.
41 H.-W. Liang, W.-J. Zhang, Y.-N. Ma, X. Cao, Q.-F. Guan, W.-P. Xu and S.-H. Yu, *ACS Nano*, 2011, **5**, 8148–8161.
42 D. M. Dotzauer, J. Dai, L. Sun and M. L. Bruening, *Nano Lett.*, 2006, **6**, 2268–2272.
43 R. Ricciardi, J. Huskens and W. Verboom, *ChemSusChem*, 2015, **8**, 2586–2605.
44 K. Kato and K. Adachi, *Modern Tribology Handbook*, vol. 1, CRC Press LLC, London, 2001.
45 S. Gu, J. Kaiser, G. Marzun, A. Ott, Y. Lu, M. Ballauff, A. Zaccone, S. Barcikowski and P. Wagener, *Catal. Lett.*, 2015, **145**, 1105–1112.
46 S. V. Jenkins, S. Chen and J. Chen, *Tetrahedron Lett.*, 2015, **56**, 3368–3372.
47 M. M. Nigra, J.-M. Ha and A. Katz, *Catal. Sci. Technol.*, 2013, **3**, 2976–2983.
48 S. Wunder, Y. Lu, M. Albrecht and M. Ballauff, *ACS Catal.*, 2011, **1**, 908–916.
49 S. Chen, S. V. Jenkins, J. Tao, Y. Zhu and J. Chen, *J. Phys. Chem. C*, 2013, **117**, 8924–8932.
50 R. He, Y.-C. Wang, X. Wang, Z. Wang, G. Liu, W. Zhou, L. Wen, Q. Li, X. Wang, X. Chen, J. Zeng and J. G. Hou, *Nat. Commun.*, 2014, **5**, 4327.
51 S. Thota, S. Chen and J. Zhao, *Chem. Commun.*, 2016, **52**, 5593.
52 M. Nemanashi and R. Meijboom, *J. Colloid Interface Sci.*, 2013, **389**, 260–267.
53 C. Deraedt, L. Salmon and D. Astruc, *Adv. Synth. Catal.*, 2014, **356**, 2525–2538.
54 R. Fenger, E. Fertitta, H. Kirmse, A. F. Thünumann and K. Rademann, *Phys. Chem. Chem. Phys.*, 2012, **14**, 9343–9349.
55 J. Zeng, Q. Zhang, J. Chen and Y. Xia, *Nano Lett.*, 2010, **10**, 30–35.
56 Y. Lu, J. Yuan, F. Polzer, M. Drechsler and J. Preussner, *ACS Nano*, 2010, **4**, 7078–7086.